

1 **Filtering effect induced by rigid massless embedded foundations**

2 by Riccardo Conti\*, Marco Morigi† & Giulia M.B. Viggiani‡

3

4 \* Associate Professor, Università Niccolò Cusano, Roma, Italy.  
5 e-mail: [riccardo.conti@unicusano.it](mailto:riccardo.conti@unicusano.it)

6

7 † PhD Student, DICII, Università di Roma Tor Vergata, Italy.  
8 e-mail: [marco.morigi@uniroma2.it](mailto:marco.morigi@uniroma2.it)

9

10 ‡ Professor, DICII, Università di Roma Tor Vergata, Italy.  
11 e-mail: [viggiani@uniroma2.it](mailto:viggiani@uniroma2.it)

12

13

14

15 Contact Author:

16 Prof. Riccardo Conti

17 Università Niccolò Cusano

18 Via Don Carlo Gnocchi, 3 - 00166 Roma, ITALY

19 e-mail: [riccardo.conti@unicusano.it](mailto:riccardo.conti@unicusano.it)

20 **Abstract**

21 It is well recognised that the dynamic interaction between structure, foundation and supporting soil  
22 can affect significantly the seismic behaviour of buildings. Among other effects, embedded and deep  
23 foundations can filter the seismic excitation, causing the foundation input motion (FIM) to differ  
24 substantially from the free-field motion. This paper presents a theoretical and numerical investigation  
25 on the filtering effect induced by rigid massless embedded foundations. Based on the results of  
26 dimensional analysis and numerical simulations, it is shown that the problem can be reasonably  
27 described by two sole dimensionless groups, namely: (i)  $\omega H/V_s$ , relating the wave length of the signal  
28 to the embedment depth of the foundation, and (ii) the aspect ratio of the foundation,  $B/H$ , where  $B$  is  
29 the foundation width in the polarization plane. New simplified and physically sound expressions are  
30 derived for the kinematic interaction factors,  $I_u = u_{\text{FIM}}/u_{\text{ff0}}$  and  $I_\theta = \theta_{\text{FIM}}H/u_{\text{ff0}}$ , which are frequency-  
31 dependent transfer functions relating the harmonic steady-state motion experienced by the foundation  
32 to the amplitude of the corresponding free-field surface motion. Standard methods for using these  
33 functions in the evaluation of the FIM are critically reviewed, with reference to both static and  
34 dynamic procedures for the seismic design of structures.

35

36

37

38 **Keywords:**

39 Soil-structure interaction; foundation input motion; free-field motion; kinematic response; embedded  
40 foundation

41

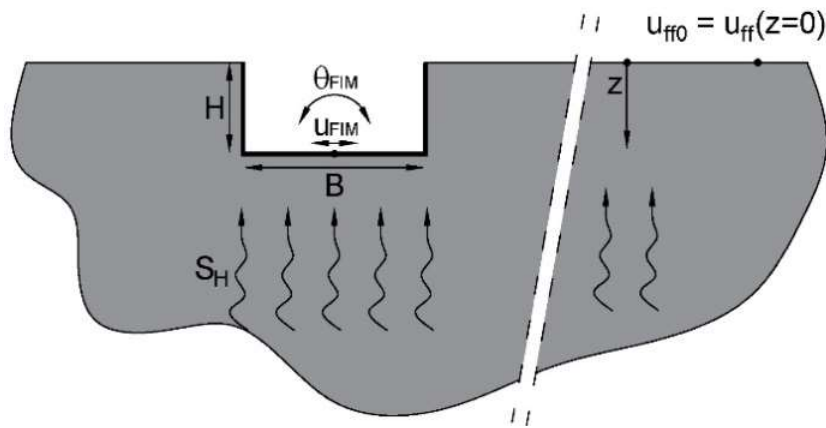
## 42 INTRODUCTION

43 The seismic performance of structures is usually evaluated under a fixed-base assumption by applying  
44 a base slab input motion equal to the free-field motion, *i.e.* neglecting the dynamic interaction  
45 between the structure, the foundation and the supporting soil (Soil-Structure Interaction, SSI).  
46 Nevertheless, the presence of a deformable soil-foundation system affects the dynamic behaviour of  
47 buildings in at least three different ways, making the seismic response of the flexibly-supported  
48 structure possibly different from that of the rigidly-supported counterpart (Bielak, 1975; Mylonakis  
49 & Gazetas, 2000): (i) it lengthens the fundamental period of the structure; (ii) it allows additional  
50 dissipation of energy into the soil by radiation and hysteresis; (iii) it filters the signal transmitted to  
51 the structure by incident waves, as a results of both base slab averaging (Veletsos *et al.*, 1997) and  
52 embedment effects (Elsabee & Morray, 1977).

53 SSI can be thought conveniently, both from a conceptual and computational point of view, as the  
54 contribution of two concurrent phenomena (Mylonakis *et al.*, 2006): (i) kinematic interaction, in  
55 which a massless foundation modifies the motion of the surrounding soil by means of its sole stiffness  
56 and (ii) inertial interaction, in which the motion of the foundation itself is further modified by the  
57 D'Alembert forces acting in the structure-foundation system. The distinction between kinematic and  
58 inertial effects, which also underlies the substructure method, provides a powerful key to  
59 interpretation of SSI problems, as observed in experimental works (Rayhani & El Nagggar, 2008),  
60 numerical works (Mahsuli & Ghannad, 2009; Politopoulos, 2010; Vega *et al.*, 2013) and field  
61 measurements (Stewart, 2000; Kim & Stewart, 2003), where many factors can affect the overall  
62 dynamic response of the structure.

63 By focusing on the filtering effect, kinematic interaction has been recognised to play a significant  
64 role in the case of both embedded (Avilés *et al.*, 2002; Politopoulos, 2010) and deep foundations (Di  
65 Laora & de Sanctis, 2013), for which the foundation input motion (FIM) can differ substantially from  
66 the free-field motion recorded at ground surface. Under the assumption of vertically propagating

67 plane shear waves, base slab averaging cannot occur and filtering effect is physically related to the  
 68 inability of the foundation elements to follow soil deformations induced by travelling waves.  
 69 In the case of rigid embedded foundations, scattering effects reduce the horizontal displacement of  
 70 the base slab,  $u_{FIM}$ , with respect to the free-field case,  $u_{ff0}$ , but can introduce a rotational component,  
 71  $\theta_{FIM}$ . This phenomenon can be described by two kinematic response factors, namely  $I_u = u_{FIM}/u_{ff0}$  and  
 72  $I_\theta = \theta_{FIM}H/u_{ff0}$ , which are frequency-dependent transfer functions relating the harmonic steady-state  
 73 motion experienced by the foundation to the amplitude of the corresponding free-field surface motion  
 74 (see Figure 1).



75  
 76 **Figure 1. Schematic representation of the soil-foundation kinematic interaction in the case of embedded**  
 77 **foundations and vertically propagating SH waves**  
 78

79 Many works in the literature have been devoted to the problem of filtering effects induced by rigid  
 80 embedded foundations, using different numerical techniques, most of them considering the case of a  
 81 massless rigid foundation – with cylindrical or rectangular shape - embedded in a uniform elastic or  
 82 viscoelastic half-space (Elsabee & Morray, 1977; Day, 1978; Dominguez, 1978; Karabalis & Beskos,  
 83 1986; Luco & Wong, 1987; Mita & Luco, 1989). More recently, Brandenburg *et al.* (2015) have  
 84 proposed a Winkler-type simplified model, relating the kinematic response factors to the translational  
 85 and rotational impedance functions for the soil.  
 86 Further studies, taking into account both the soil-foundation system and the superstructure (complete  
 87 SSI), have shown that the filtering effect is usually beneficial for squat structures while it may  
 88 increase the ductility demand in the case of slender buildings with deeply embedded foundations or

89 basements (Mahsuli & Ghannad, 2009). Moreover, in the case of base isolated structures, such as  
 90 nuclear plants, where standard devices have isolation capacity only in the horizontal plane, the  
 91 dynamic response of non-isolated modes can be significantly amplified by rocking oscillations of the  
 92 foundation (Politopoulos, 2010; Politopoulos *et al.*, 2015).

93 The filtering effect induced by embedded foundations is usually described using the formulas  
 94 proposed by Elsabee & Morray (1977):

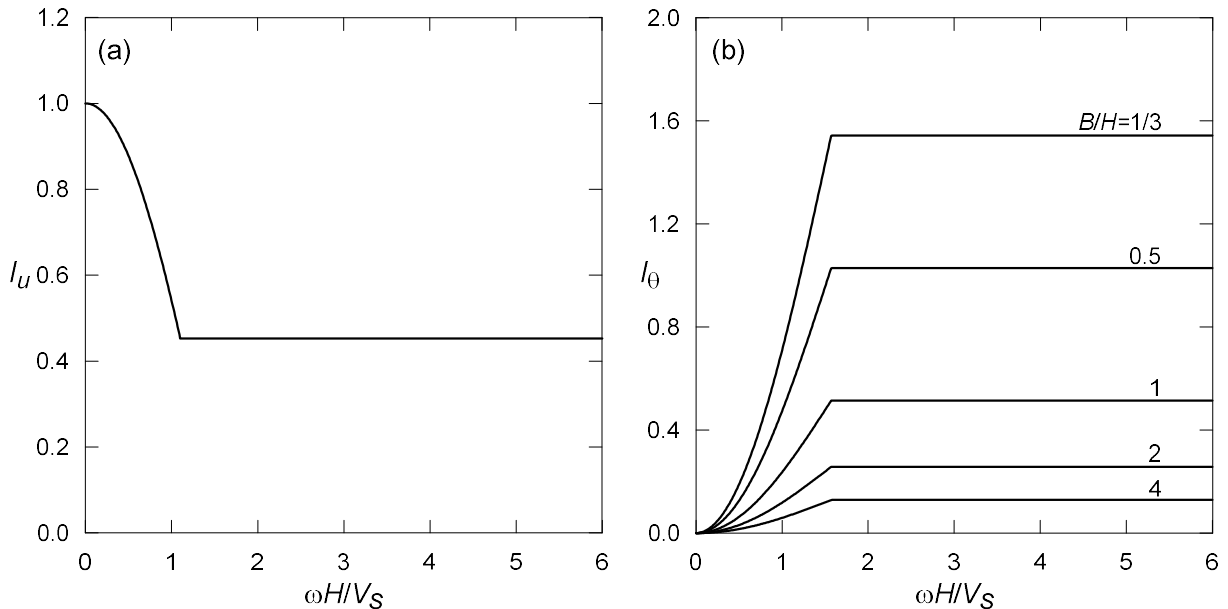
$$95 \quad I_u = \frac{u_{FIM}}{u_{ff0}} = \begin{cases} \cos\left(\frac{\omega H}{V_S}\right) & \omega \leq 0.7 \frac{\pi V_S}{2 H} \\ 0.453 & \omega > 0.7 \frac{\pi V_S}{2 H} \end{cases} \quad (1)$$

$$96 \quad I_\theta = \frac{\theta_{FIM} \cdot H}{u_{ff0}} = \begin{cases} \frac{2H}{B} 0.257 \left[1 - \cos\left(\frac{\omega H}{V_S}\right)\right] & \omega \leq \frac{\pi V_S}{2 H} \\ \frac{2H}{B} 0.257 & \omega > \frac{\pi V_S}{2 H} \end{cases} \quad (2)$$

97 where  $B$  is the foundation width,  $\omega$  is the angular frequency of the excitation and  $V_S$  is the shear wave  
 98 velocity of the supporting soil (FEMA 440, 2005; Mylonakis *et al.*, 2006).

99

100



101

102

103

**Figure 2. Formulas proposed by Elsabee & Morray (1977) for the kinematic response factors: (a)  $I_u$  and (b)  $I_\theta$**

104

105 As shown in Figure 2, despite their simplicity these equations provide a quite crude approximation  
 106 of the actual physical phenomenon, essentially relating the motion of the rigid foundation to the  
 107 translation of the free-field at the foundation level (Eq. (1)) and to the so-called free-field “pseudo-  
 108 rotation”, resulting from the differential displacement of the soil in the embedment region (Eq. (2)).  
 109 This paper presents a numerical and theoretical investigation of the filtering effect induced by rigid  
 110 massless embedded foundations. The goal of this study is threefold: (i) to offer insight into the  
 111 relevant factors affecting the problem; (ii) to extend the numerical observations available in the  
 112 literature; (iii) to define new simplified, but physically sound, solutions to be incorporated in  
 113 recommendations for the seismic design of structures with embedded foundations. Results of this  
 114 work will be useful not only to improve the understanding of the mechanisms underlying filtering  
 115 effects, such as the little relevance of the three-dimensional features of the foundation, but also for  
 116 the design practice.

117

## 118 **PROBLEM DEFINITION AND DIMENSIONAL ANALYSIS**

119 In this section we derive the dimensionless groups governing the filtering effect induced by embedded  
 120 foundations, under the assumption of vertically propagating plane shear waves. We refer to the  
 121 general case of a rectangular foundation (embedment depth  $H$ , width  $B$ , length  $L$ , mass density  $\rho^*$ ,  
 122 shear modulus  $G^*$ , damping ratio  $\xi$ ) embedded in a homogeneous isotropic visco-elastic soil layer  
 123 (depth  $H_d$ , mass density  $\rho$ , shear modulus  $G$ , Poisson’s ratio  $\nu$ , damping ratio  $\xi$ ). Table 1 summarises  
 124 the 14 physical variables relevant for the problem at hand, which can be formulated as:

$$\begin{aligned}
 125 \quad u_{FIM} &= f(u_{ff0}, \omega, H, B, L, \rho^*, G^*, \rho, G, \xi, \nu, H_d) \\
 \theta_{FIM} &= g(u_{ff0}, \omega, H, B, L, \rho^*, G^*, \rho, G, \xi, \nu, H_d)
 \end{aligned}
 \tag{3}$$

126

127 **Table 1. Variables governing the dynamic interaction between soil and embedded foundations**

	variable	dim.	description
foundation	$u_{FIM}$	L	base horizontal disp.
input	$\theta_{FIM}$	$L^0$	rotation

free-field motion	$u_{ff0}$ $\omega$	L $T^{-1}$	surface horizontal disp. angular frequency
foundation properties	$\rho^*$	$ML^{-3}$	mass density
	$G^*$	$MT^{-2}L^{-1}$	shear modulus
	H	L	embedment
	B	L	width
	L	L	length
soil properties	$\rho$	$ML^{-3}$	mass density
	G	$MT^{-2}L^{-1}$	shear modulus
	$\nu$	$L^0$	Poisson's ratio
	$\xi$	$L^0$	damping ratio
	$H_d$	L	depth of soil deposit

128

129 Applying the Buckingham theorem, it is possible to rescale Equations (3) in dimensionless form,  
 130 using  $H$ ,  $G$  and  $\rho$  as dimensionally independent variables:

$$\begin{aligned}
 I_u &:= \frac{u_{FIM}}{u_{ff}} = F\left(\frac{\omega H}{V_S}, \frac{\rho^*}{\rho}, \frac{G^*}{G}, \frac{B}{H}, \frac{L}{H}, \frac{H_d}{H}, \xi, \nu\right) \\
 I_\theta &:= \frac{\theta_{FIM} H}{u_{ff0}} = G\left(\frac{\omega H}{V_S}, \frac{\rho^*}{\rho}, \frac{G^*}{G}, \frac{B}{H}, \frac{L}{H}, \frac{H_d}{H}, \xi, \nu\right)
 \end{aligned} \tag{4}$$

132 The dimensionless ratios in Equations (4) take into account the physical, mechanical and geometrical  
 133 properties of the problem. Among these,

- 134 (i)  $\omega H/V_S$  relates the embedment depth of the foundation to the wavelength of the excitation  
 135 ( $\lambda = V_S/f = 2\pi V_S/\omega$ ), *i.e.* the deeper the foundation the longer the wavelengths which can  
 136 be filtered by scattering effects;
- 137 (ii)  $G^*/G$  and  $\rho^*/\rho$  are the relative shear stiffness and mass density, respectively, between the  
 138 foundation and the soil: the stiffer and the denser the foundation, the stronger its filtering  
 139 capacity;
- 140 (iii)  $H_d/H$  is the relative depth between the soil deposit and the foundation embedment, which,  
 141 for soil layers of finite depth, can introduce spurious oscillations in the kinematic  
 142 interaction factors (Elsabee & Morray, 1977);

143 In order to reduce the problem at hand and/or in the light of a kinematic-inertial decomposition  
 144 method, some simplifying assumptions are usually introduced in the literature, *i.e.*: the embedded  
 145 foundation is rigid ( $G^*/G \gg 1$ ) and massless ( $\rho^*/\rho \ll 1$ ); the soil deposit is assimilated to a  
 146 homogeneous half-space ( $H_d/H \gg 1$ ). As far as  $\xi$  and  $\nu$  are concerned, numerical works have shown  
 147 that, while affecting the dynamic response of both the foundation and the soil, they have a minor  
 148 influence on the kinematic response factors (Mita & Luco, 1989; Di Laora & de Sanctis, 2013).  
 149 Moreover, it will be shown in the following that, as far as the aspect ratios of the foundation are  
 150 concerned, only the foundation width  $B$  in the polarization plane of the shear wave affects  
 151 significantly the filtering phenomenon. Under these assumptions, the interaction factors can be  
 152 expressed as functions of two sole parameters:

$$\begin{aligned}
 I_u &= F\left(\frac{\omega H}{v_s}, \frac{B}{H}\right) \\
 I_\theta &= G\left(\frac{\omega H}{v_s}, \frac{B}{H}\right)
 \end{aligned}
 \tag{5}$$

154 By introducing a further hypothesis on the foundation geometry, two limiting 1D conditions can be  
 155 identified, *i.e.*:

156 (i)  $B/H = 0$  (infinitely thin foundation): the difference between the FIM and the  
 157 corresponding free-field surface motion is related only to the variation of ground motion  
 158 with depth. As a consequence, the two kinematic interaction factors can be computed with  
 159 reference to the free-field motion in the embedment region, assuming elastic behaviour  
 160 for the soil ( $\xi = 0$ ), as:

$$\begin{aligned}
 I_u|_{(B/H=0)} &= \frac{u_{ff}|_{z=H}}{u_{ff0}} = \cos\left(\frac{\omega H}{v_s}\right) \\
 I_\theta|_{(B/H=0)} &= \frac{\theta_{ff} \cdot H}{u_{ff0}} = 1 - \cos\left(\frac{\omega H}{v_s}\right)
 \end{aligned}
 \tag{6}$$

162 where  $\theta_{ff} = (u_{ff0} - u_{ff}|_{z=H})/H$  is the free-field pseudo-rotation of the soil.

163 (ii)  $B/H = \infty$  (infinitely extended foundation): the foundation cannot rotate ( $\theta_{FIM} = 0$ ) and the  
 164 half-space condition results in  $u_{FIM} = u_{ff0}$ . As a consequence, the two kinematic  
 165 interaction factors reduce to:



166 
$$\begin{aligned} I_u|_{(B/H=\infty)} &= 1 \\ I_\theta|_{(B/H=\infty)} &= 0 \end{aligned} \tag{7}$$

167 These asymptotic conditions will be used in the following both to interpret numerical results and to  
 168 provide simplified solutions for design.

169

170 **NUMERICAL ANALYSES**

171 A total of 17 plane-strain analyses of a rectangular foundation of width  $B$  and depth  $H$ , embedded in  
 172 an homogeneous half-space, were carried out in the time domain using the finite difference code  
 173 FLAC 2D v7 (Itasca, 2011). Moreover, two three-dimensional analyses were carried out with the  
 174 code FLAC 3D. The complete set of analyses is reported in Table 2, with the ratio  $B/H$  ranging from  
 175 0.25 to 20.

176

177 **Model definition**

178 Figure 2 shows the typical mesh adopted in this study. The soil was modelled as a linear visco-elastic  
 179 isotropic material, with mass density  $\rho = 1.835 \text{ t/m}^3$ , shear wave velocity  $V_s = 100 \text{ m/s}$  and Poisson  
 180 ratio  $\nu = 0.3$ . A Rayleigh viscous damping was used, with a given value of 2 % at the reference  
 181 frequencies of 1 Hz and 10 Hz.

182

183 **Table 2. Summary of the numerical analyses**

#	$H$ [m]	$B$ [m]	$B/H$	$L/B$	$B_m$ [m]	$H_m$ [m]
1	12	3	0.25	$\infty$	300	27
2	12	6	0.5	$\infty$	300	27
3	3	3	1	$\infty$	300	27
4	6	6	1	$\infty$	300	27
5	12	12	1	$\infty$	300	27
6	3	6	2	$\infty$	300	27
7	6	12	2	$\infty$	300	27
8	12	24	2	$\infty$	300	27
9	3	12	4	$\infty$	300	27
10	6	24	4	$\infty$	300	27
11	12	48	4	$\infty$	450	27
12	3	18	6	$\infty$	300	27

13	6	36	6	$\infty$	450	27
14	12	72	6	$\infty$	450	27
15	3	30	10	$\infty$	450	27
16	6	60	10	$\infty$	450	27
17	3	60	20	$\infty$	450	27
18	6	6	1	1	100	27
19	6	12	2	1	100	27

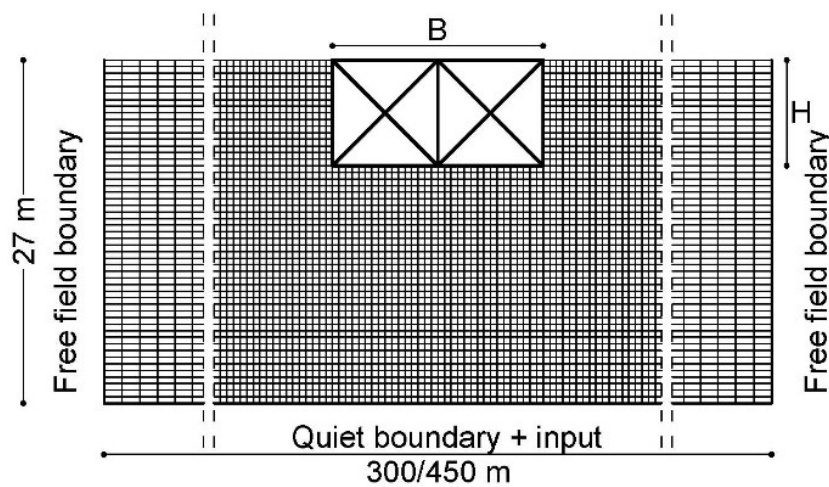
184

185 The rigid massless foundation was modelled as an open excavation with rigid boundaries and  
186 supports, in order to enforce rigid body displacements. To this purpose, elastic beams with reduced  
187 mass density were introduced ( $E = 5.0 \text{ GPa}$ ,  $A = 7.0 \text{ m}^2$ ,  $I = 6.0 \text{ m}^4$ ,  $\rho_b = 0.008 \text{ t/m}^3$ ), both along the  
188 boundaries of the foundation and as an internal frame, thus increasing the overall shear stiffness of  
189 the foundation without affecting significantly its total mass. Perfect contact was assumed between the  
190 sidewalls and the soil elements.

191 Free-field boundary conditions were applied along the lateral sides of the mesh, involving the  
192 coupling of the main grid with a one-dimensional free-field column through viscous dashpots, in such  
193 a way that outward waves originating from the interior of the model can be properly absorbed.

194 As far as the boundary condition at the base of the mesh is concerned, both viscous dashpots and the  
195 dynamic input were applied in order to reproduce the upward propagation of shear waves within a  
196 semi-infinite domain (Joyner & Chen, 1975). The input was a constant amplitude sinusoidal sweep,  
197 defined in terms of a horizontal displacement time history, with a duration of 60 s and a frequency  
198 increasing linearly with time from 0.5 to 10 Hz. This range was chosen to include the typical  
199 frequency content of real earthquakes.

200



201

202

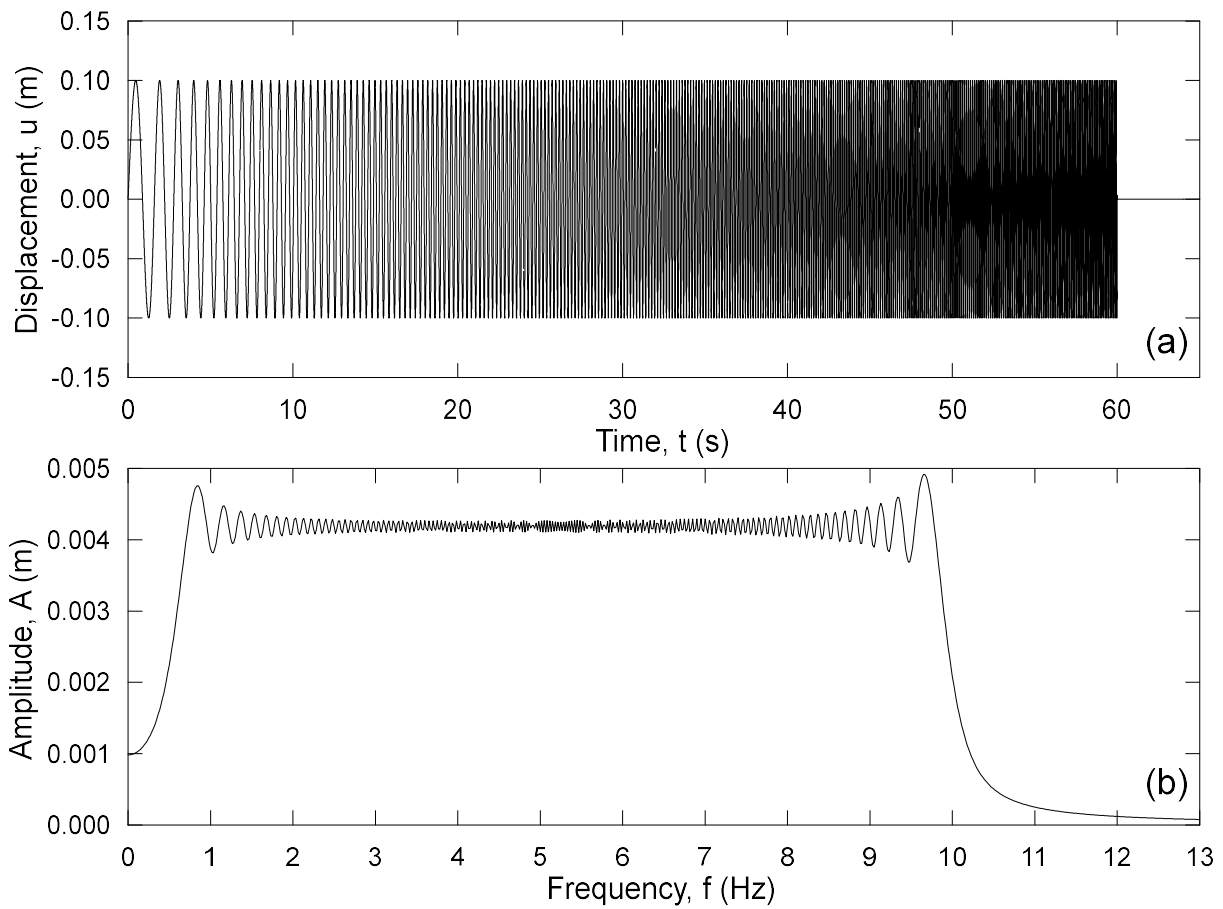
203

Figure 3. 2D analyses: finite difference model

204 The dimensions of the mesh were chosen after a preliminary parametric study so as to minimise  
205 possible side effects due to spurious wave reflections at boundaries, and hence to recover free field  
206 conditions. The elements of the mesh have a maximum size of 0.75 m close to the foundation, in  
207 order to describe correctly the minimum wavelength of the applied signal ( $\lambda_{\min}=V_s/f_{\max} = 10$  m).  
208 Moving to 3D analyses, the square foundation ( $B/L=1$ ) was modelled as an empty excavation, with  
209 shell elements of increased stiffness and reduced mass density attached to the internal boundaries.  
210 The numerical model is consistent with that adopted in the 2D analyses, in terms of boundary  
211 conditions, dynamic input, mesh discretisation, and mechanical properties of both soil and foundation  
212 elements.

213

214



215

216

217

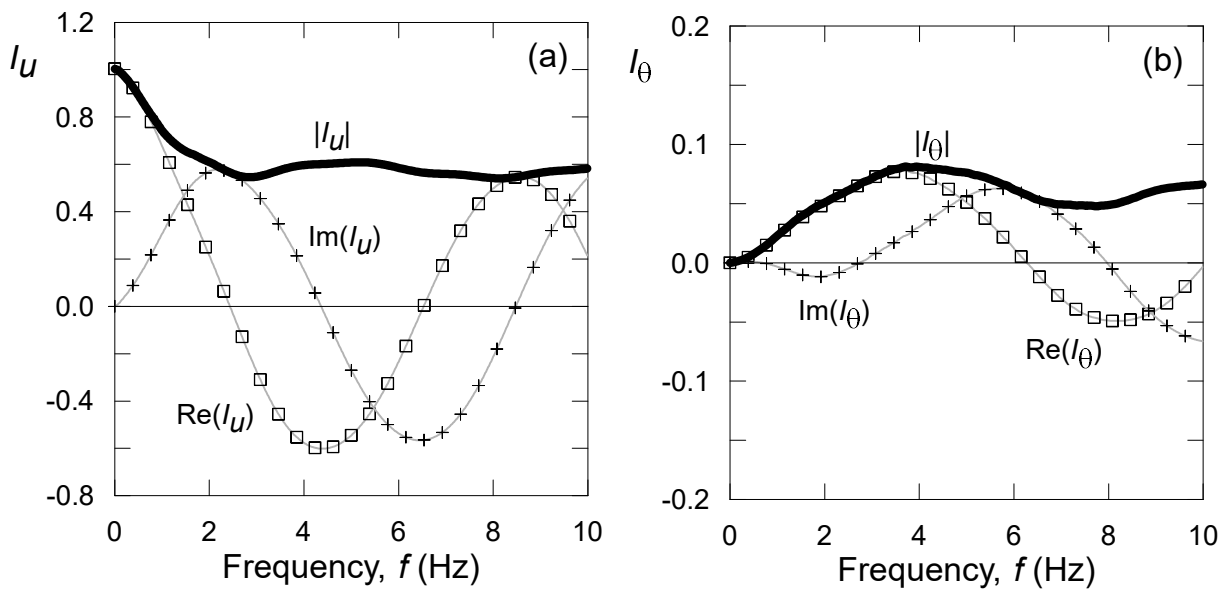
**Figure 4. Sweep input signal: (a) displacement time history and (b) Fourier amplitude spectrum**

218

219 **Results**

220 The complex valued functions  $I_u$  and  $I_\theta$  were obtained from the Fourier transform of  $u_{ff0}(t)$ ,  $u_{FIM}(t)$   
 221 and  $\theta_{FIM}(t)$ , where  $u_{FIM}$  corresponds to the horizontal displacement of the bottom centre of the  
 222 foundation and  $\theta_{FIM}$  is computed as  $(v_1-v_2)/B$ , where  $v_1$  and  $v_2$  are the vertical displacements of the  
 223 two corners at the base of the foundation. As an example, Figure 3 shows, for analysis No. 11, the  
 224 numerical values of the real part, imaginary part and amplitude of (a)  $I_u$  and (b)  $I_\theta$ .

225



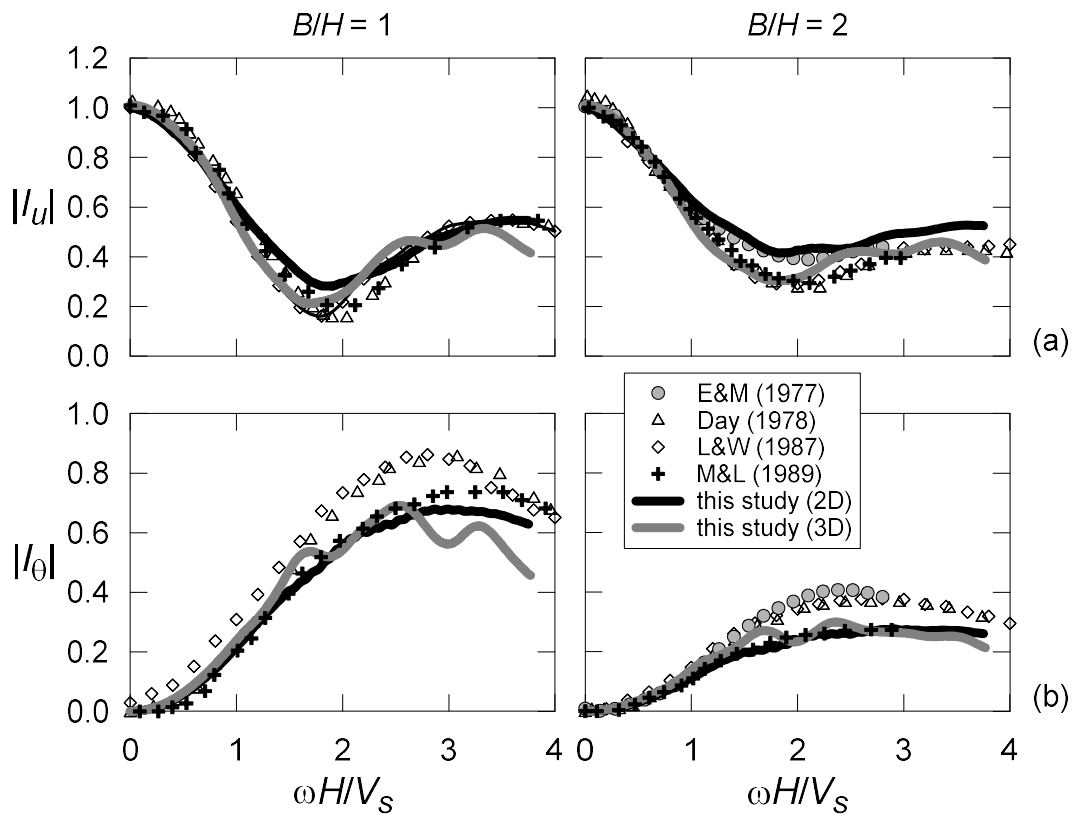
226

227 **Figure 5. Analysis No. 11: Real and imaginary part of the kinematic interaction factors: (a)  $I_u$  and (b)  $I_\theta$**

228

229 In order to ascertain three-dimensional effects on the filtering problem, Figure 4 compares the results  
 230 from this study ( $B/H = 1, 2$  and  $L/B = 1, \infty$ ), in terms of (a)  $|I_u|$  and (b)  $|I_\theta|$ , with some of those available  
 231 in the literature, obtained with BEM, FEM or hybrid BEM-FEM approaches. All literature results  
 232 refer to the case of cylindrical (Day, 1978; Luco & Wong, 1987) and square (Mita & Luco, 1989)  
 233 foundations ( $L/B=1$ ) embedded in a uniform elastic half-space, with the only exception of Elsabee &  
 234 Morray (1977), who considered a cylindrical foundation embedded in an elastic soil layer of finite  
 235 depth overlying a rigid bedrock. In spite of showing some scatter, numerical data are in substantial  
 236 agreement, both qualitatively and quantitatively, with a maximum difference of  $\pm 15\%$  on the average  
 237 in terms of  $I_\theta$  ( $B/H = 2$ ). Moreover, FDM results are in perfect agreement with each other and with

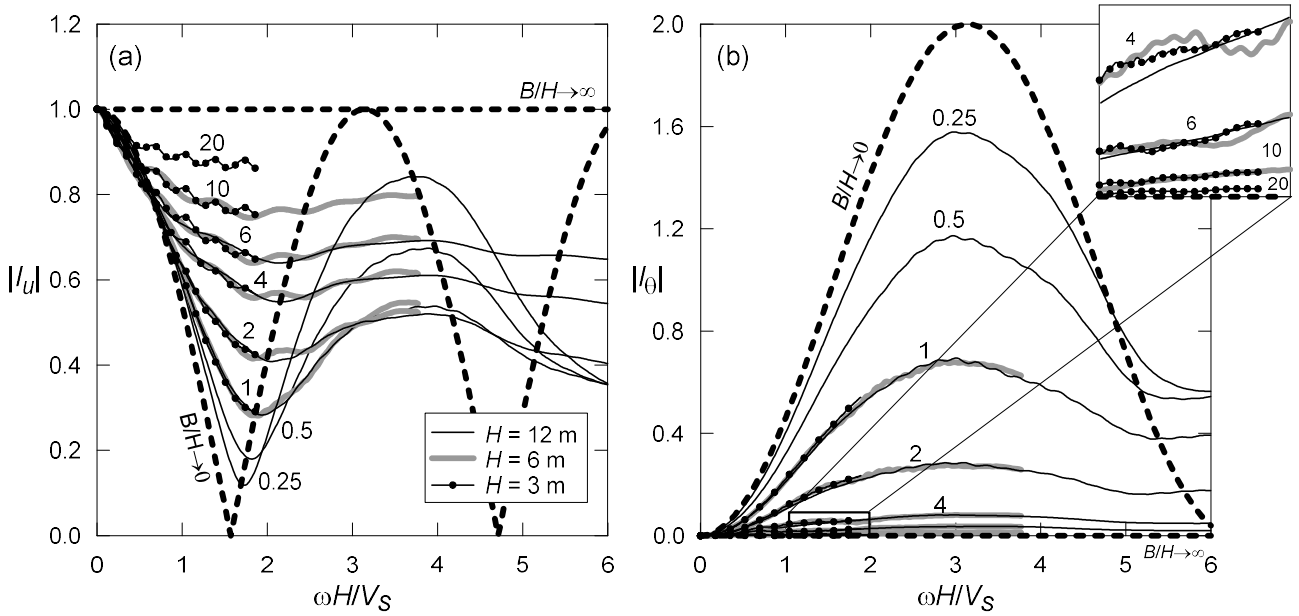
238 those reported by Mita & Luco (1989). Based on this comparison, it is apparent that the ratio  $L/H$  has  
 239 a minor influence on the kinematic interaction factors, with respect to  $\omega H/V_S$  and  $B/H$ , and, therefore,  
 240 that it can be ignored without any loss of relevant information. This implies that, when looking at  
 241 filtering effects, 2D analyses provide a reasonable representation of the 3D behaviour of rigid  
 242 embedded foundations.  
 243



244  
 245 **Figure 6. Comparison between numerical FDM results ( $B/H = 1, 2$ ) and literature data, in terms of: (a)  $|I_u|$  and**  
 246 **(b)  $|I_\theta|$**   
 247

248 Figures 5 shows the numerical values of (a)  $|I_u|$  and (b)  $|I_\theta|$ , as a function of the dimensionless  
 249 frequency  $\omega H/V_S$  and for different values of  $B/H$ , together with the theoretical solutions for the 1D  
 250 limit conditions of  $B/H = 0$  and  $B/H = \infty$ . For small  $B/H$  (squat/slender foundations), the interaction  
 251 factors tend to the free-field 1D conditions, where filtering effects are mostly due to the embedment  
 252 of base slab. In this condition,  $|I_u|$  shows an oscillating trend, with local minima and maxima clearly  
 253 related to the resonant frequencies of the corresponding free-field case, and a significant rocking

254 component emerges in the FIM, as reflected by  $|I_\theta|$ . On the other hand, for large  $B/H$  values (spread  
 255 foundations), both factors tend to stabilize, moving towards the asymptotic solution for  $B/H = \infty$ ,  
 256 without significant oscillations as  $\omega H/V_s$  increases. As a result, filtering of the horizontal  
 257 displacements reduces, but no rocking component is introduced. In other words, numerical analyses  
 258 indicate that both  $I_u$  and  $I_\theta$  are strongly affected by the aspect ratio of the foundation and are not  
 259 related merely to the embedment depth of the foundation. In particular, for a given value of  $H$ , the  
 260 larger the foundation the smaller the overall filtering effect induced on the free-field ground motion.  
 261



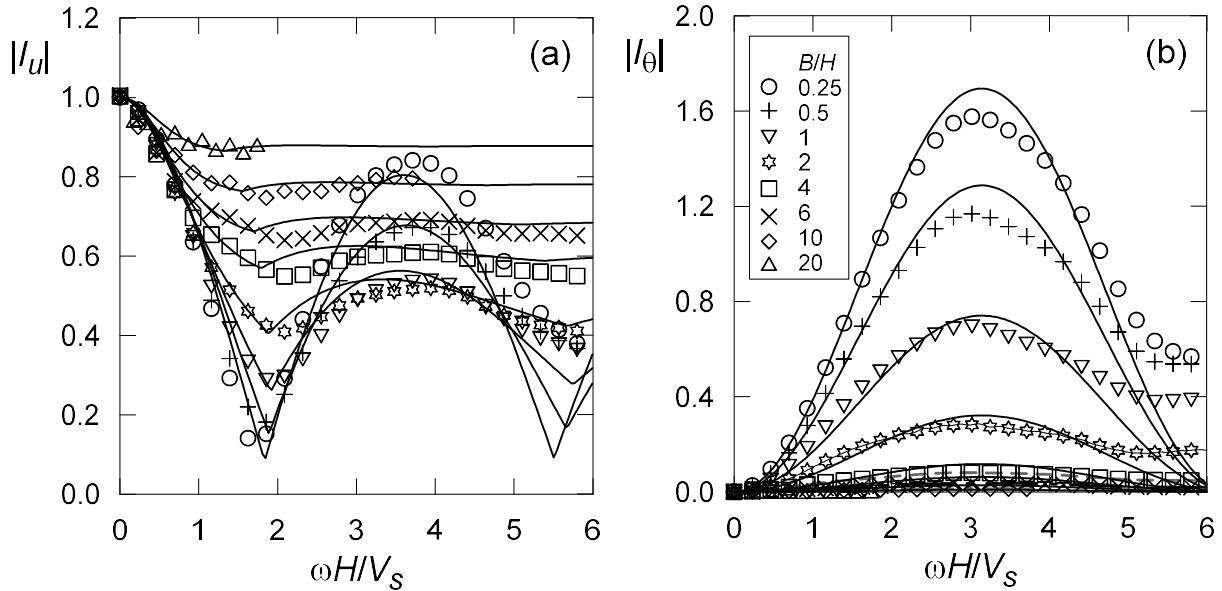
262  
 263 **Figure 7. Numerical results and limit conditions of: (a)  $|I_u|$  and (b)  $|I_\theta|$**   
 264

265 Based on the best fit of numerical data, simplified expressions for  $|I_u|$  and  $|I_\theta|$  were defined using *ad*  
 266 *hoc* functions which allow to recover the 1D limiting conditions as  $B/H \rightarrow 0$  or  $B/H \rightarrow \infty$ :

$$267 \quad \left| I_u \left( \frac{\omega H}{v_s}, \frac{B}{H} \right) \right| = a_1 \frac{1 + a_2 \left( \frac{\omega H}{v_s} \right)^2}{1 + \left( \frac{\omega H}{v_s} \right)^2} + (1 - a_1) \frac{|\cos(a_3 \frac{\omega H}{v_s})|}{\left[ 1 + \left( \frac{\omega H}{v_s} \right)^2 \right]^{2a_1}} \quad (8)$$

$$268 \quad \left| I_\theta \left( \frac{\omega H}{v_s}, \frac{B}{H} \right) \right| = a_4 \left[ 1 - \cos \left( \frac{\omega H}{v_s} \right) \right] \quad (9)$$

269 in which coefficients  $a_1, a_2, a_3, a_4$  depend on the ratio  $B/H$ , as detailed in Appendix. As shown in  
 270 Figure 6, Equations (8) and (9) provide a good description of the actual trend exhibited by  $|I_u|$  and  $|I_\theta|$ ,  
 271 particularly for  $\omega H/V_S < 5$ , which corresponds to the range of frequencies typical of real earthquakes.  
 272



273  
 274 **Figure 8. Comparison between numerical results (symbols) and interpolating functions (lines): (a)  $|I_u|$  and (b)  $|I_\theta|$**   
 275

276 **GUIDELINES FOR DESIGN**

277 In the light of the results presented so far, and bearing in mind that the accuracy of any simplified  
 278 method should be consistent with the uncertainties involved in the characterization of the free-field  
 279 ground motion, this section aims to review critically standard guidelines for including filtering effects  
 280 in the evaluation of the FIM (FEMA 440, 2005; Mylonakis *et al.*, 2006). We will refer to both  
 281 dynamic and static procedures for the seismic design of structures, where the design earthquake is  
 282 defined in terms of a time history or a response spectrum, respectively.

283 Since the interaction factors are complex valued transfer functions, the mathematical rigorous  
 284 procedure for computing the FIM consists in applying  $I_u$  and  $I_\theta$  to the Fourier spectrum of the free-  
 285 field motion, when the latter is defined as a time history (Method M1). However, taking into account  
 286 that simplified formulas are available only for real-valued functions  $|I_u|$  and  $|I_\theta|$ , the latter are adopted



287 in the design practice, ignoring any possible phase shift between the translation and rocking  
 288 components of the foundation motion (Method M2).

289 Moving to static procedures, Mylonakis *et al.* (2006) suggested to apply  $|I_u|$  and  $|I_\theta|$  directly to the  
 290 free-field acceleration spectrum ( $S_{a,ff0}(\omega)$ ), if the design earthquake is specified in this form  
 291 (Method M3). Accordingly, for a structural mass located at a vertical distance  $H_c$  from the base,  
 292 foundation rocking and translation result in:

$$293 \quad S_{a,FIM}(\omega) = [|I_u(\omega)| + |I_\theta(\omega)| \cdot H_c/H] S_{a,ff0}(\omega) . \quad (10)$$

294 Clearly, methods M2 and M3 involve quite crude simplifications, whose effects must be ascertained.

295 To this end, we considered the ideal case of an embedded foundation ( $H = 6$  m,  $B/H = 1, 4$  and  $6$ ,  
 296  $V_S = 100$  m/s), supporting a structural mass located at  $H_c = 20$  m and subjected to ten acceleration  
 297 time histories, all registered during real earthquakes. For sake of simplicity, we considered the above  
 298 accelerations as free field surface accelerations ( $\ddot{u}_{ff0}$ ), that is we ignored any stratigraphic  
 299 amplification effects. Table 3 summarizes the values of peak acceleration, *PGA*, duration,  $T_{5-95}$  and  
 300 mean frequency,  $f_m$ . Figure 7 shows (a) the acceleration time histories and (b) the Fourier amplitude  
 301 spectra, while Figure 8 shows the elastic response spectra at 5 % damping of the ten signals.

302

303

#	Earthquake	PGA [g]	$T_{5-95}$ [s]	$f_m$ [Hz]
1	Kocaeli - Turkey (1999)	0.34	17.6	2.67
2	Loma Prieta - USA (1989)	0.37	15.7	4.11
3	Friuli - Italy (1976)	0.32	4.8	3.98
4	Imperial Valley - USA (1979)	0.33	10.3	4.34
5	Hollister - USA (1961)	0.19	9.2	2.84
6	Kobe - Japan (1995)	0.33	18.6	4.11
7	Trinidad - USA (1983)	0.17	3.2	4.30
8	Northridge - USA (1983)	0.58	19.0	3.38
9	Chi Chi – Taiwan (1999)	0.21	9.4	4.23
10	Landers - USA (1992)	0.44	22.3	5.72

304

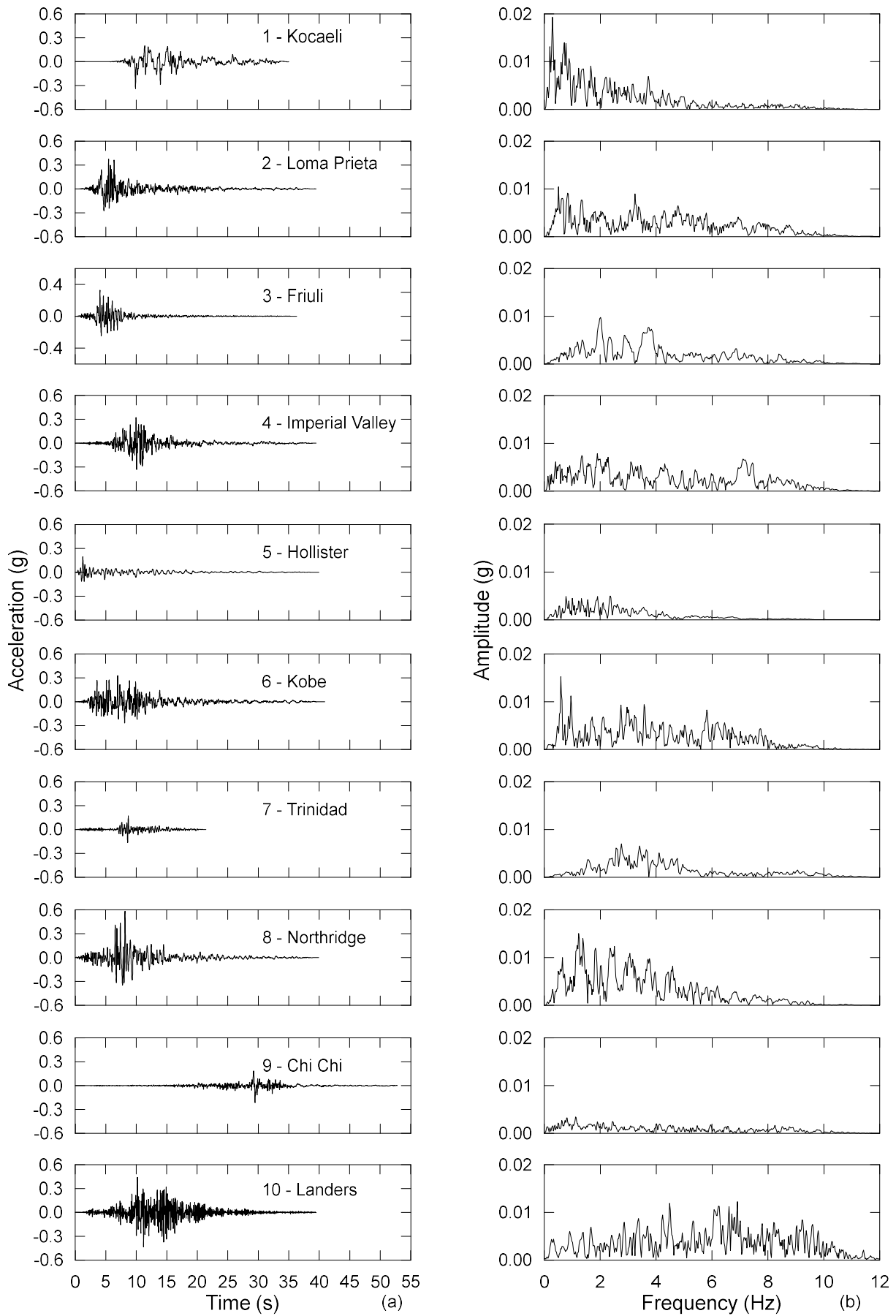


Figure 9. Ten real earthquakes: (a) acceleration time histories and (b) Fourier amplitude spectra

305  
306  
307

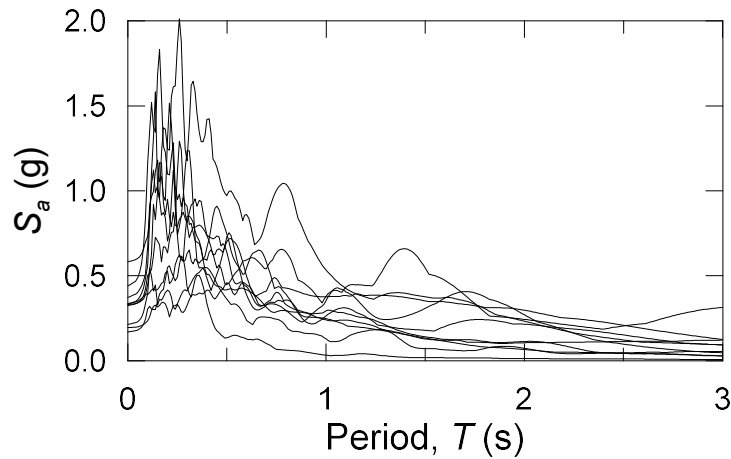


Figure 10. Ten real earthquakes: elastic response spectra

308  
309  
310

311 Figure 9 shows, for earthquake No.7 and for  $B/H = 1$  and 4: (a, b) the acceleration time histories and  
 312 (c) the elastic response spectrum at 5% damping of both free-field motion and FIM, the latter  
 313 computed according to methods M1 and M2. As expected, filtering effects depend strongly on the  
 314 ratio  $B/H$ , with a maximum reduction of about 50 % in the horizontal peak acceleration computed for  
 315  $B/H = 1$ , together with the appearance of a significant rocking component. Looking at the response  
 316 spectra of Figure 9(c), the combined effect of translation and rotation of the foundation turns out to  
 317 be either beneficial or detrimental for the structural system, depending on the ratio  $B/H$ , the major  
 318 effects arising in the short period range. For the case at hand ( $H_c = 20\text{m}$ ), procedure M1 provides a  
 319 maximum amplification in the spectral ordinates of 65 % for  $B/H = 1$  and a maximum reduction of  
 320 40 % for  $B/H = 4$ , with respect to the free-field condition. By comparing the results from methods  
 321 M1 and M2, no substantial difference is observed in terms of maximum accelerations, the only  
 322 difference being a phase shift in the time history. Moreover, neglecting phase angles in the  
 323 computation of the FIM introduces only small errors in the spectral ordinates, with a maximum value  
 324 of 25 % for structural periods larger than 0.2 s ( $B/H = 4$ ), always on the conservative side. These  
 325 observations apply to all the earthquakes considered in this work.

326

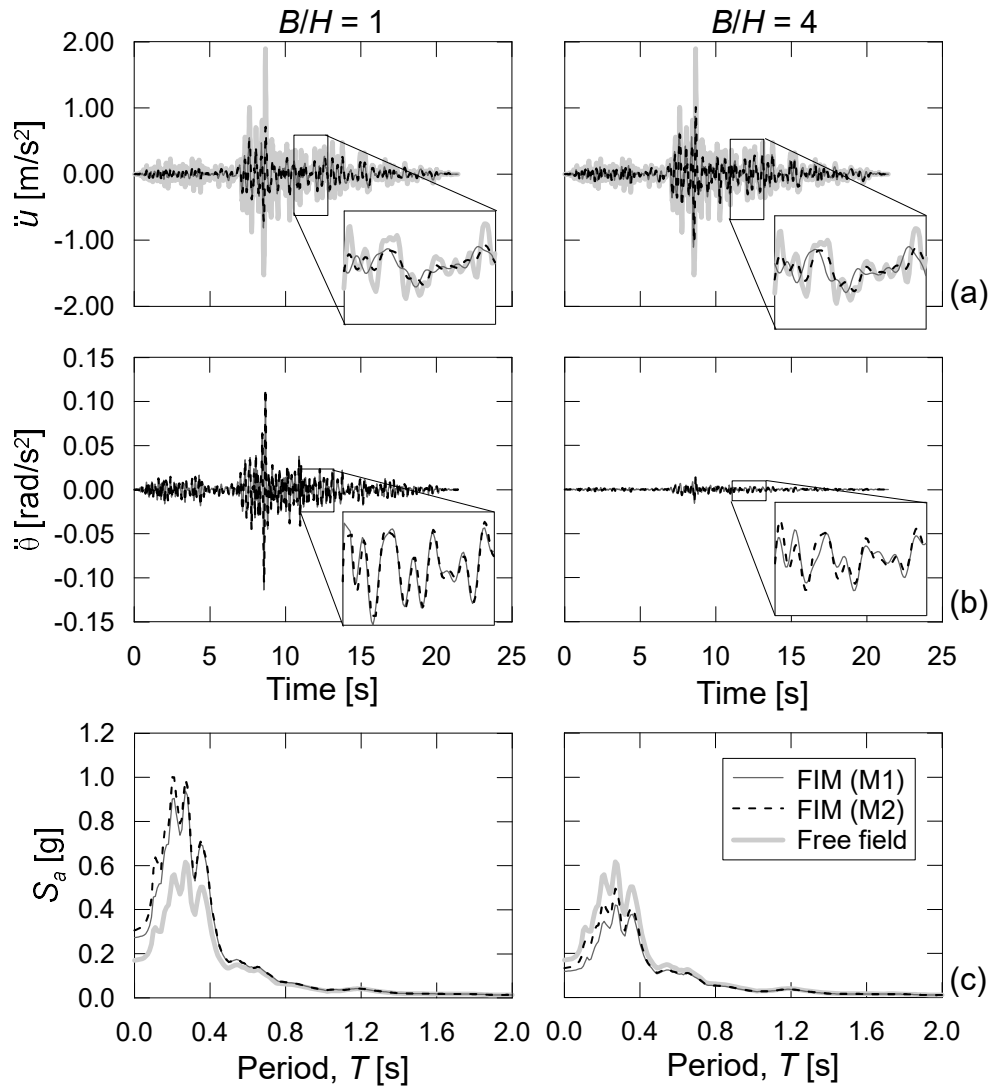


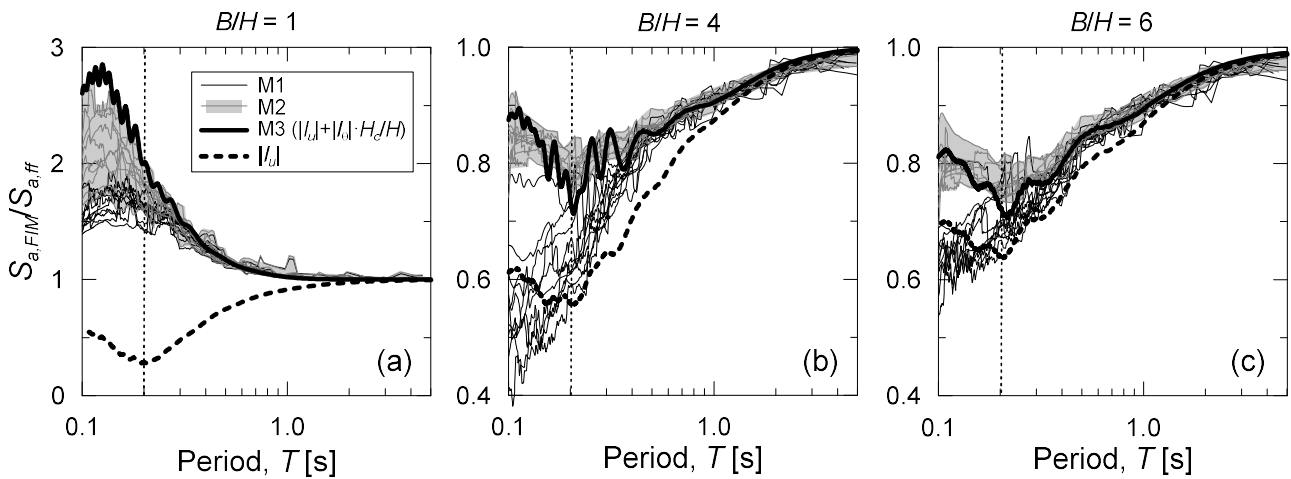
Figure 11. Earthquake No. 7 - acceleration time histories of: (a) horizontal translation and (b) rocking of free-field motion and FIM, together with (c) their elastic response spectra.

327  
328  
329  
330

331 Figure 10 shows, for all earthquakes and for  $B/H = 1, 4$  and  $6$ , the ratio of FIM to free-field response  
332 spectral ordinates, the former computed according to methods M1 and M2. The figure shows also the  
333 values  $|I_u| + |I_\theta| \cdot H_c/H$  (method M3), and those of  $|I_u|$ , to highlight errors in reducing the design spectrum  
334 of the free-field motion without taking into account  $|I_\theta|$ . Depending on the ratio  $B/H$ , *i.e.* on the  
335 interplay between the reduction in the horizontal motion and the introduction of rocking oscillations,  
336 kinematic interaction may lead to either an increase ( $B/H = 1$ ) or a reduction ( $B/H = 4, 6$ ) of the  
337 spectral ordinates, with respect to the free-field case. Both simplified procedures M2 and M3 allow  
338 to take into account these effects, providing always conservative results with respect to the rigorous  
339 procedure M1. However, the error introduced reduces with increasing periods, where the foundation

340 rocking tends to vanish and, for  $T > 0.2$  s - i.e. for most of the real structures where considering the  
 341 filtering effect induced by the foundation embedment makes sense - the maximum error associated  
 342 to methods M2 and M3 is 35 % and 40 % respectively. On the other hand, in spite of being always  
 343 unconservative, using solely  $|I_u|$  provides a reasonable approximation of the actual trend for large  
 344 values of  $B/H$  ( $B/H \geq 4$ ), where the foundation rocking is small.

345



346

347 **Figure 12. All earthquakes: ratio of the response spectra between FIM and free-field motion for: (a)  $B/H = 1$ , (b)**  
 348  **$B/H = 4$  and (c)  $B/H = 6$  ( $H = 6$  m,  $H_c = 20$  m,  $V_s = 100$  m/s).**

349

350 Based on the above observations, it can be concluded that both procedures M2 and M3 can be adopted  
 351 effectively in the design practice, when computing the design motion either as a time history or as an  
 352 elastic response spectrum, to take into account in a simplified manner filtering effects induced by  
 353 embedded foundations.

354

### 355 CONCLUSIONS

356 This work was devoted to the filtering effects induced by rigid massless embedded foundations  
 357 subjected to vertically propagating shear waves. Based on results from dimensional analysis and  
 358 numerical simulations, it was found that the problem can be reasonably described solely by two  
 359 dimensionless groups, namely: (i)  $\omega H/V_s$ , relating the wave length of the signal to the embedment

360 depth of the foundation, and (ii) the aspect ratio of the foundation,  $B/H$ , where  $B$  is the foundation  
 361 width in the polarization plane.

362 New simplified and physically sound expressions were derived for the kinematic interaction factors,  
 363  $|I_u|$  and  $|I_\theta|$ , and standard methods for using these functions in the evaluation of the FIM were critically  
 364 reviewed, with reference to both static and dynamic procedures for the seismic design of structures.

365 More in detail, it was pointed out that real-valued functions  $|I_u|$  and  $|I_\theta|$  can be used instead of complex-  
 366 valued factors  $I_u$  and  $I_\theta$ . Moreover, filtering functions can be applied either to the Fourier amplitude  
 367 spectrum or to the response spectrum of the free-field signal, if the design motion must be specified  
 368 as a time history or acceleration spectrum respectively.

369 In order to reduce the problem, usual approximations of linear viscoelastic material and uniform half-  
 370 space were assumed for the soil. Possible nonlinearities or non-uniformities, leading to variability of  
 371 shear wave velocity with induced strain level or depth, could be taken into account using conventional  
 372 procedures, as summarized in Brandenberg *et al.* (2015).

373 Further studies are needed to explore the filtering behaviour of embedded foundations in subsoil  
 374 conditions substantially different from those considered in this paper and to highlight the role of the  
 375 stiffness of the foundation in cases where the rigidity assumption is no longer applicable.

376

## 377 APPENDIX

378 Coefficients  $a_1, a_2, a_3, a_4$  in Equations (8) and (9) are computed as a function  $B/H$  from the best fit of  
 379 numerical data:

$$380 \quad a_1(B/H) = \frac{(B/H)^\alpha}{\beta + (B/H)^\alpha} \quad \alpha = 1.04 \quad \beta = 4.24 \quad (A1)$$

$$381 \quad a_2(B/H) = \frac{\alpha + (B/H)}{1 + (B/H)} \quad \alpha = 1.92 \quad (A2)$$

$$382 \quad a_3(B/H) = \frac{1}{1 + \sqrt{B/H}} + \alpha(B/H)^\beta \quad \alpha = 0.32 \quad \beta = 0.38 \quad (A3)$$

$$383 \quad a_4(B/H) = \frac{1}{1 + \alpha(B/H)^\beta} \quad \alpha = 1.70 \quad \beta = 1.62 \quad (A4)$$

384

385

386 **Acknowledgements**

387 The work presented in this paper was developed with the financial support of the Italian Department  
388 of Civil Protection within the ReLUIIS research project.

389

390 **References**

- 391 Avilés J., Suarez M., Sanchez-Sesma F.J. (2002). “Effects of wave passage on the relevant dynamic  
392 properties of structures with flexible foundation”. *Earthquake. Engng. Struct. Dyn.*, 31, 139-159.
- 393 Bielak J. (1975). “Dynamic behavior of structures with embedded foundations”. *Earthquake. Engng.*  
394 *Struct. Dyn.*, 3, 259-274.
- 395 Brandenberg S.J., Mylonakis G., Stewart J. (2015). “Kinematic Framework for Evaluating Seismic  
396 Earth Pressures on Retaining Walls”. *J. Geotech. Geoenviron. Eng.*, 141(7), 04015031.
- 397 Day S.M. (1978). “Seismic response of embedded foundations”. Proc. ASCE Convention, Chicago,  
398 IL, October, Preprint No. 3450.
- 399 Di Laora R., de Sanctis L. (2013). “Piles-induced filtering effect on the Foundation Input Motion”.  
400 *Soil Dyn. Earthquake Eng.*, 46, 52-63
- 401 Dominguez J. (1978). “Response of embedded foundations to travelling waves”. Report R78-24,  
402 Dept. of Civ. Engrg., Mass. Inst, of Tech., Cambridge, Mass.
- 403 Elsabee F., Morray J. P. (1977). “Dynamic behavior of embedded foundation”. Rep. No. R77-33,  
404 Dept. of Civil Engineering, Massachusetts Institute of Technology, Cambridge, Mass.
- 405 FEMA 440 (2005). “Improvement of nonlinear static seismic analysis procedures”. Federal  
406 Emergency Management Agency, Washington, DC.
- 407 Itasca (2011). *FLAC Fast Lagrangian Analysis of Continua v.7.0*. User’s Manual.
- 408 Joyner W.B., Chen A.T.F. (1975). “Calculation of nonlinear ground response in earthquakes”. *Bull.*  
409 *Seism. Soc. Am.*, 65, 1315-1336.
- 410 Karabalis D.L., Beskos D.E. (1986). “Dynamic response of 3-D embedded foundations by the  
411 boundary element method”. *Comput. Methods Appl. Mech. Eng.*, 56, 91-119.

412 Kim S., Stewart J. (2003). "Kinematic Soil-Structure Interaction from Strong Motion  
413 Recordings". *J. Geotech. Geoenviron. Eng.*, 129(4), 323-335.

414 Luco J.E., Wong H.L. (1987). "Seismic response of foundations embedded in a layered half-space".  
415 *Earthquake. Engng. Struct. Dyn.*, 15, 233-247.

416 Mahsuli M., Ghannad M.A. (2009). "The effect of foundation embedment on inelastic response of  
417 structures". *Earthquake. Engng. Struct. Dyn.*, 38(4), 423-37.

418 Mita A., Luco J.E. (1989). "Impedance functions and input motions for embedded square  
419 foundations". *Journal of Geotechnical Engineering*, ASCE, 115, 491-503.

420 Mylonakis G., Gazetas G. (2000). "Seismic soil-structure interaction: beneficial or detrimental?".  
421 *Journal of Earthquake Engineering*, 4(3), 277-301.

422 Mylonakis G., Nikolaou S., Gazetas G. (2006). "Footings under seismic loading: Analysis and design  
423 issues with emphasis on bridge foundations". *Soil Dyn. Earthquake Eng.*, 26(9), 824-853.

424 Politopoulos I. (2010). "Response of seismically isolated structures to rocking type excitations".  
425 *Earthquake. Engng. Struct. Dyn.*, 39, 325-42.

426 Politopoulos I., Sergis I., Wang F. (2015). "Floor response spectra of a partially embedded seismically  
427 isolated nuclear plant". *Soil Dyn Earthquake Eng.*, 78, 213-217.

428 Rayhani M.H.T., El Naggar M.H. (2008). "Numerical modeling of seismic response of rigid  
429 foundation on soft soil". *Int J Geomech.*, 8, 336-46.

430 Stewart J.P. (2000) "Variations between foundation-level and free-field earthquake ground motions".  
431 *Earthquake Spectra*, 16, 511-532.

432 Vega J., Aznárez J.J., Santana A., Alarcón E., Padrón L.A., Pérez J.J., Maeso O. (2013). "On soil-  
433 structure interaction in large non-slender partially buried structures". *Bull Earthquake Eng.*, 11,  
434 1403-1421.

435 Veletsos A.S., Prasad A.M., Wu W.H. (1997). "Transfer functions for rigid rectangular foundations".  
436 *Earthquake. Engng. Struct. Dyn.*, 26, 5-17.